Manipulation of Competitive Growth for Particle Size Control in Emulsion Polymerization

Vincenzo Liotta, Christos Georgakis,* E. David Sudol, and Mohamed S. El-Aasser

Chemical Process Modeling and Control Research Center, Emulsion Polymers Institute, and Department of Chemical Engineering, Lehigh University, Bethlehem, Pennsylvania 18015

The utility of the growth mechanism to influence relative particle growth is investigated in a semi-batch reactor. A dynamic competitive growth model is developed and used to simulate the growth of two monodisperse polystyrene particle populations (bidisperse system) at 50 °C. Validation of the model with on-line density and on-line particle diameter measurements demonstrates that radical absorption into particles is more likely to occur by a collision mechanism than either by a propagation or diffusion mechanism. Experimental and simulation results show that relative narrowing of the bidisperse system increases as the weight fraction polymer inside the particles (W_p) decreases. It is concluded that the ability to alter W_p in a semi-batch reactor makes this mode of operation attractive for particle size distribution control.

Introduction

The product of a conventional emulsion polymerization results from a free radical polymerization of monomer dissolved in aqueous-based polymer particles. Industrial applications of these dispersed particles include synthetic rubber, adhesives, paints, and medical products. The particle size distribution (PSD) of these latexes is an important product characteristic due to its influence over the end-use properties including mechanical strength, opacity, and viscosity. Once a certain PSD is linked to a desired property, controlling the PSD toward the appropriate final form becomes an important objective.

In this work, the utility of the growth mechanism to influence the relative breadth of a discrete form of the PSD (bidisperse system) is investigated in a semi-batch reactor. After introducing the concept of relative diameter growth, a dynamic competitive growth model is developed for a styrene/polystyrene system and validated with experimental data from an automated reactor control facility. In the latter sections, simulation and experimental results show how process conditions can be manipulated to influence the relative growth of the bidisperse system.

Relative Particle Growth

The goal of this paper is to investigate the extent to which a distribution's relative breadth can be controlled by using competitive growth. Assuming growth from a seed distribution is the only operative mechanism, the breadth of the particle distribution can be altered only if different-sized particles grow at different rates. This is the essence of competitive growth. Vanderhoff and co-workers were the first to investigate this phenomenon using two monodisperse populations of particles (bidisperse system) under batch conditions (Vanderhoff and Bradford, 1956; Vanderhoff et al., 1956). The work presented in this paper is an extension of that earlier work. Emphasis here is placed on the *dynamics* of competitive growth and ways that it can be influenced in a semi-batch reactor.

* To whom correspondence should be addressed. Iacocca Hall, 111 Research Dr., Bethlehem, PA 18015. Phone: (610)-758-5432. E-mail: cg00@Lehigh.edu.

It is imperative at this point to recognize the different competitive growth representations that exist. For instance, the choice to characterize a distribution with either diameter or volume is critical since Chen and Wu (1988) point out that, under typical growth conditions, the standard deviation of a distribution decreases with time if diameter is used and increases with time if volume is used. To remain consistent with the work of Vanderhoff and co-workers, particle diameters are considered in this work.

For a distribution of particles, one must also distinguish between absolute breadth (represented by standard deviation) and relative breadth (represented by standard deviation divided by the mean). Such distinctions can also be applied to the case where monodisperse populations of particles are of concern instead of a full distribution. As demonstrated elsewhere (Poehlein and Vanderhoff, 1973), consider a general expression for the volume growth rate of a polymer in a particle as

$$\frac{\mathrm{d}V}{\mathrm{d}t} = K_a D^c = K_b [M]_p \bar{n} \tag{1}$$

where V and D are the volume and diameter of an unswollen latex particle, respectively, and K_a and K_b are different proportionality constants. The second half of eq 1 is the more familiar form where $[M]_p$ is the monomer concentration in the particle and $\bar{n}$ is the average number of radicals per particle. Rearrangement of the first half of eq 1 in terms of diameter yields:

$$\frac{1}{D}\frac{\mathrm{d}D}{\mathrm{d}t} = \frac{2K_a}{\pi} D^{c-3} \tag{2}$$

The important relative growth indicator, $\mathrm{d}D/D$ (relative rate of diameter growth), as written here, is dependent on its size, D, raised to the $c - 3$ power. Inspection of eq 2 shows that if $c = 3$, the relative diameter rate is independent of its size. If $c < 3$, smaller particles will grow faster in diameter than larger ones, in a relative sense, and the distribution will narrow. Finally, if $c > 3$ the distribution will broaden in relative terms. After integrating eq 2 from initial to final particle diameters for two different-sized monodisperse populations, Figure 1 results (Vanderhoff and Bradford, 1956). Subscript 2 denotes the larger sized population,

S0888-5885(96)00643-4 CCC: $14.00

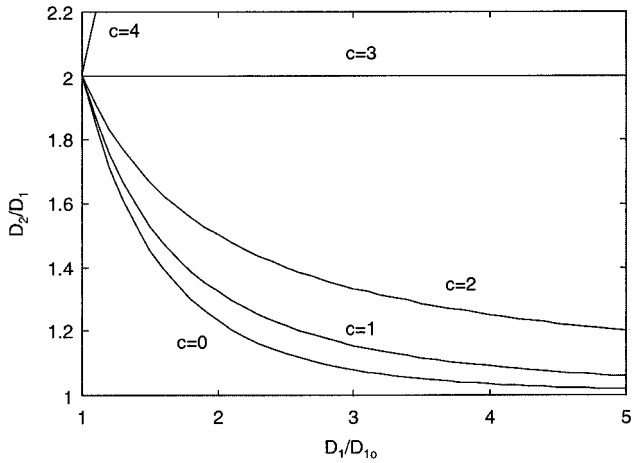

Figure 1. Relative diameter growth of a bidisperse system for different orders of volume growth, c (Vanderhoff and Bradford, 1956).

subscript 1 denotes the smaller sized population, and subscript o denotes the initial size. The importance of this plot is that it draws a connection between a distribution's relative breadth evolution and relative diameter growth of a bidisperse system. An increasing diameter ratio as shown in Figure 1 represents relative PSD broadening ($c > 3$), while a decreasing diameter ratio represents relative narrowing of a distribution ($c < 3$). Thus, the diameter ratio of the bidisperse system can be viewed as a relative growth indicator. In this paper, the relationship between the evolution of the diameter ratio and the order of volume growth, c, is investigated.

Vanderhoff and co-workers determined the value for c in a batch reactor by performing competitive growth experiments. Two monodisperse populations of different-sized polystyrene seeds were grown at various initiator concentrations, monomer/polymer ratios, emulsifier amounts, and temperatures. The generation of new particles was suppressed by maintaining the surfactant concentration below the critical micelle concentration. Their results showed that, for particles larger than 150 nm and by using a water-soluble persulfate initiator, $c = 2.5$ (relative narrowing of the PSD) provided a good fit to the data. They also found that, for particles less than 150 nm, the value of c varied from 1 to close to 0. Therefore, under batch conditions, c is a function of particle size below 150 nm, but then reaches a constant value equal to 2.5 for particles with diameters greater than 150 nm.

The conclusion from the above study was that competitive growth characteristics are fixed under batch conditions. This is not too surprising since there were no real manipulated variables to influence the process evolution in their study. Once the recipe was chosen and charged into the reactor, the reaction was limited to one specific particle monomer concentration trajectory. At the onset of the reaction, the monomer concentration in the particles was at its highest, and either remained constant until monomer droplets had disappeared or continually decreased as the reaction progressed (below the monomer saturation limit). The effect of keeping the monomer concentration at a particular value for an extended period of time was not studied (except at the saturation value). Furthermore, measurements of the relative breadth of the system were taken only at the end of the polymerization which say little of the dynamics of the system. It is, thus, plausible that the 2.5 power that was determined is an averaged global effect. Local dynamics must be investigated to determine under what conditions this order of volume growth can be made to change. This is the topic of the next section.

Influence of Process Conditions on Relative Diameter Growth. The idea that competitive growth can be influenced through semi-batch operation comes from an understanding of how particles of different sizes can be made to grow at different rates. For the purpose of discussion, consider the ratio of differential volume growth for two particles:

$$\frac{dV_2}{dV_1} = \frac{[M]_{p_2}}{[M]_{p_1}} \frac{\bar{n}_2}{\bar{n}_1} \tag{3}$$

The assumption that the monomer concentration in the particles is a negligible function of particle size is a good one (as will be shown later), and so $[M]_{p_2}/[M]_{p_1} \approx 1$. Thus, different-sized particles will grow at different volume rates only if they have a different average number of radicals. If $\bar{n}_1 = \bar{n}_2$, then the particle *volume* growth rates are equal and the smaller particles approach the larger particles in *diameter*. This relative narrowing effect decreases as the ratio $\bar{n}_2/\bar{n}_1$ increases until a value for the ratio is reached when the particle diameters begin to move away from each other in a relative sense. Using the latter half of eq 1 and assuming a constant relative growth (i.e., $c = 3$), the condition under which this occurs can be determined:

$$\frac{\bar{n}_2}{\bar{n}_1} > \left(\frac{D_2}{D_1}\right)^3 \tag{4}$$

Thus, the key to influencing relative diameter growth is the ability to change the ratio $\bar{n}_2/\bar{n}_1$ at will. A simple calculation will show how such a situation is possible. For a typical aqueous phase radical concentration, negligible radical desorption, and assuming radical absorption follows a diffusion mechanism, a direct calculation of $\bar{n}$ for varying process conditions can be made. The basis of the calculation is a simple, but good approximation (Ugelstad and Hansen, 1976) of the Stockmayer−O'Toole solution:

$$\bar{n} = (0.25 + \alpha_a/2)^{1/2} \tag{5}$$

where $\alpha_a = \sigma V_s N_a/k_t$. In this equation, σ is the radical absorption rate, V_s is the swollen particle volume, N_a is Avogadro's number, and k_t is the termination rate coefficient. Given the above assumptions, a calculation of $\bar{n}$ as a function of W_p and the swollen particle diameter can be made. The results are shown in Figure 2. By picking two different particle diameters on this plot, one can see the effect that W_p has on the $\bar{n}_2/\bar{n}_1$ ratio. For a large amount of monomer in the particles (low W_p), $\bar{n}$ remains close to 0.5 throughout the diameter range in Figure 2. As W_p increases, the ratio increases, and thus, relative narrowing decreases.

The influence that W_p has on relative growth stems from the relationship between W_p and the gel effect. At high W_p values, the gel effect (decrease in k_t) becomes more severe. Since the impact of the gel effect (autoacceleration) is greater for larger particles, they will have a much larger average number of radicals than smaller particles. Thus, $\bar{n}_2/\bar{n}_1$ increases as W_p increases. Alternatively, at low W_p values, the gel effect is less important, so that $\bar{n}$ values in larger particles are not inflated. The result is lower $\bar{n}_2/\bar{n}_1$ ratios. Process

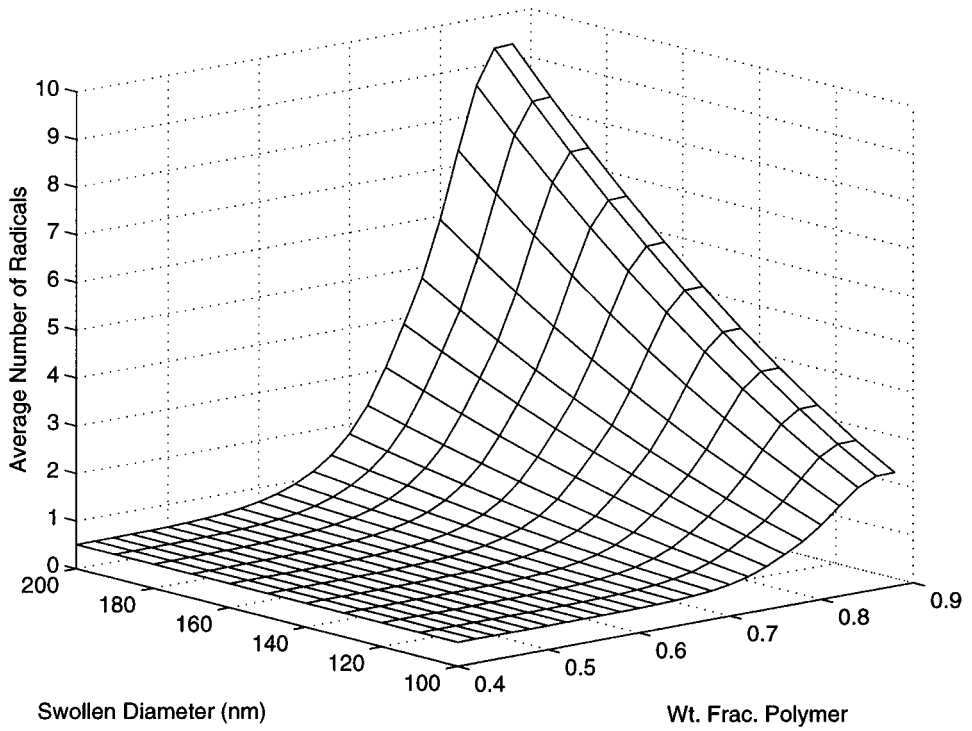

Figure 2. The effect of particle polymer weight fraction and particle diameter on the average number of radicals per particle using eq 5.

variables which effectively influence W_p provide a handle on influencing relative growth evolution. Changing the monomer feed rate to the reactor is an effective way to alter W_p. Provided that there is enough monomer to satisfy the reaction, increasing the monomer feed rate will decrease W_p. The relationship between monomer feed and relative growth evolution is considered in greater detail later on in this work.

The preceding calculation shows that, for a simplified situation, competitive growth characteristics can be influenced by process conditions. Researchers have investigated more general versions of this example in dimensionless form. Ugelstad et al. (1973) studied the influence of dimensionless radical absorption and desorption parameters on the order of volume growth, c, for water-soluble initiators. They concluded that the maximum value for c is 2 for systems that exhibit low or negligible radical desorption (the case here). They explained Vanderhoff's result of $c = 2.5$ as consistent with a system exhibiting significant radical desorption and reabsorption into the particles. It must be noted, however, that the conclusions of the work of Ugelstad et al. (1973) depend on the assumption that radicals absorb on the basis of a diffusion mechanism, and are not valid if this is not true.

More recently, Mork (1995) performed a similar study with oil-soluble initiators. In this case, the investigation results were more general because radical entry and exit coefficients were formulated in terms of power laws with respect to diameter. Stationary state $\bar{n}$ results were shown, in general, to be qualitatively similar to water-soluble initiator results.

In both of the above investigations, the researchers acknowledged that their calculation procedures resulted in instantaneous values. In reality, mechanistic events depend on conversion or particle size, and so the order of volume growth is likely to change during the polymerization. In order to simulate such a situation, both studies applied their stationary state equations in an evolutionary manner via a stepwise calculation. The validity of such a procedure to simulate a dynamic system depends on the assumption that the steady-state values for the average number of radicals per particle are reached instantaneously. However, as Mork (1995) pointed out in the same study, reaching steady-state values of $\bar{n}$ may be a slow process in systems where rates of radical desorption are very small. Thus, for our system, where radical desorption rates are small and the kinetics are expected to vary, a truly dynamic simulation is required.

A dynamic model, presented in the next section, fulfills this requirement. Once validated with on-line data, the model is used to further the discussion presented in this section. That is, an investigation quantifying the influence of process conditions on relative growth evolution is carried out.

Dynamic Competitive Growth Model

A dynamic competitive growth model was developed to simulate the homopolymerization of styrene under the following reactor condition assumptions.

(1) A bidisperse latex seed is used.

(2) The number of particles is constant.

(3) The reactor is run under semi-batch conditions with neat monomer feed.

(4) The reactor is run isothermally at 50 °C.

(5) No monomer droplets exist.

(6) The volumes of the separate phases are additive.

(7) The monomer concentration (or weight fraction polymer or volume fraction monomer) inside the particles, $[M]_p$ (or W_p or ϕ_m), is not a function of particle diameter.

(8) The styrene monomer is negligibly soluble in the aqueous phase.

Some of the preceding assumptions are valid under specific conditions. For instance, the second assumption is good if particle nucleation and aggregation is minimized through appropriate surfactant content. Ensuring that a proper mixing environment exists and that

the monomer saturation limit of the particles is not exceeded make the fifth assumption valid. The last assumption is motivated by the use of styrene.

The seventh assumption deserves some special attention. The fact that this assumption is only valid in a specific regime can be shown through a simple thermodynamic calculation. By assuming an equilibrium between the partial molar free energy of monomer, free energy of mixing, and the interfacial energy contribution and assuming a high polymer molecular weight value (Morton et al., 1954), one can arrive at eq 6.

$$\frac{2\gamma}{r}\frac{\mathrm{MW_m}}{\rho_m R_g T^\circ} + [1 - \phi_m + \ln \phi_m + \chi(1-\phi_m)^2] = \ln \frac{[M]_w}{[M]_{sat}} \quad (6)$$

where γ is the interfacial tension between the particle and the aqueous phase, r is the particle radius, $\mathrm{MW_m}$ is the molecular weight of the monomer, R_g is the gas constant, T° is the temperature, χ is the Flory−Huggins interaction parameter, $[M]_w$ is the aqueous phase monomer concentration, and $[M]_{sat}$ is the aqueous monomer concentration at saturation. The numerical solution to eq 6 (at the saturated condition) as a plot of ϕ_m versus r for different values of χ and γ is given by Ugelstad and Hansen (1976). Their plot shows that, under most conditions, ϕ_m is a weak function of particle radius except at small swollen particle radii < 40 nm. This insensitivity increases as $[M]_w$ decreases, or proportionately, as the equilibrium monomer concentration inside the particles decreases. Thus, in our work, where particle diameters are greater than 90 nm and the monomer concentration in the particles is always below the saturation limit, assumption 7 holds.

Model Equations. Given the above assumptions, reactor balances in the form of ordinary differential equations (ODEs) can be written for the bidisperse system. It is important to note that in all subsequent equations, the subscript i denotes population 1 or 2, so that when this notation is used, two equations exist for the one presented. Also, subscripts 1 and 2 refer to parameters associated with populations 1 and 2, respectively. A description and appropriate units for all the variables can be found in the nomenclature section.

Equation 7 is the rate of change of the total reactor volume, V_r, or equivalently, the increase in the total monomer swollen particle volume, V_p (population 1 and 2), with time. It depends on the volume increase due to the monomer feed and the change in volume due to reaction in population 1 and 2. The next equation (8) is a material balance on the total moles of monomer in the reactor $\{[M]_p V_p\}$ and accounts for the monomer moles fed into the reactor, F_m, and the monomer disappearance due to reaction. Equation 9 is an account of how the diameter ratio of the bidisperse system, the principal output of the model, changes with time. This equation can be readily derived from the two equations describing the diameter evolution of each monodisperse species. The next ODE (10), accounts for the total mass of monomer added to the reactor, M_{add}. Keeping track of this variable helps relate outputs like W_p to instantaneous conversion, X. The last balance (11) accounts for the total moles of initiator in the reactor $\{[I]V_w\}$. This equation can be solved analytically, if needed, to reduce the order of the system.

$$\frac{dV_r}{dt} = \frac{dV_p}{dt} = \frac{F_m(\mathrm{MW_m})}{\rho_m} + (R_{p_1} + R_{p_2})V_r(\mathrm{MW_m})\left(\frac{1}{\rho_p} - \frac{1}{\rho_m}\right) \quad (7)$$

$$\frac{d\{[M]_p V_p\}}{dt} = F_m - (R_{p_1} + R_{p_2})V_r \quad (8)$$

$$\frac{d\{D_2/D_1\}}{dt} = \frac{R_{p_2}V_r(\mathrm{MW_m})N_{t_1}/N_{t_2} - R_{p_1}(D_2/D_1)^3}{3(D_2/D_1)^2 V_{p_1}(1-\phi_m)\rho_p} \quad (9)$$

$$\frac{dM_{add}}{dt} = F_m \mathrm{MW_m} \quad (10)$$

$$\frac{d\{[I]V_w\}}{dt} = -k_d[I]V_w \quad (11)$$

In the above equations, $\mathrm{MW_m}$ is the monomer molecular weight, ρ_m and ρ_p are the monomer and polymer densities, and k_d and is the initiator decomposition rate coefficient. The polymerization rate for a given population, R_{p_i}, can be written as

$$R_{p_i} = \frac{k_p \bar{n}_i [M]_p N_{t_i}}{N_a V_r} \quad (12)$$

where k_p is the propagation rate coefficient, $\bar{n}_i$ is the average number of radicals per particle for a given population, $[M]_p$ is the monomer concentration inside the particles, and N_{t_i} is the total number of particles of population i in the reactor. The principal unknowns in the rate equation are the propagation rate coefficient, k_p, and both average number of radicals per particle, $\bar{n}_1$ and $\bar{n}_2$.

Under most conditions, the propagation rate coefficient, k_p, does not change with time and is equal to the propagation rate coefficient at zero conversion, k_{p0}. However, at high conversions when the polymer inside the particles becomes glassy, a diffusion limitation becomes prevalent and must be taken into account. Below a certain critical free volume, v_{fmc}, Sundberg et al. (1981), have described the propagation rate coefficient relation by

$$\ln \frac{k_p}{k_{p_0}} = B\left(\frac{1}{v_{fmc}} - \frac{1}{v_f}\right) \quad (13)$$

where the free volume in the particles, v_f, can be expressed in terms of the monomer volume fraction inside the particles, ϕ_m, and monomer and polymer contributions to the free volume, v_{fm} and v_{fp}, respectively:

$$v_f = v_{fm}\phi_m + v_{fp}(1-\phi_m) \quad (14)$$

Soh and Sunberg (1982) provided semi-empirical relations to obtain both v_{fm} and v_{fp} as a function of temperature, T, for several systems including polystyrene:

$$v_{fm} = 0.112 + 6.2 \times 10^{-4} T \quad (15)$$

$$v_{fp} = 0.0245 + 1.4 \times 10^{-4}(T - 82) \quad (16)$$

In comparison to the propagation rate coefficient, the average number of radicals per particle is much more difficult to predict. The next section outlines the variables which influence $\bar{n}$ and the associated equations.

The average number of radicals per particle depends on complex phenomena including the absorption of radicals into the particles, the desorption of radicals from the particles, and their termination in the particles. Li and Brooks (1993) have determined that the balance for the average number of radicals per particle follows a differential equation of the following form:

$$\frac{d\bar{n}_i}{dt} = \sigma_i - k_i\bar{n}_i - \frac{f_i k_t}{V_{s_i} N_a}\bar{n}_i^2 \tag{17}$$

where σ_i is the radical absorption rate, k_i is the desorption rate coefficient, V_{s_i} is the swollen particle volume (all for population i), and k_t is the termination rate coefficient. The coefficient, f_i, in the above equation depends on the relative magnitudes of σ_i, k_i, and k_t in the following manner:

$$f_i = \frac{2(2\sigma_i + k_i)}{2\sigma_i + k_i + \dfrac{k_t}{V_{s_i} N_a}} \tag{18}$$

To complete the picture, events in the aqueous phase must also be taken into account. Both populations of particles need to be considered when obtaining the aqueous phase radical concentration, $[R]_w$, found via a solution of the following radical balance while evoking a quasi-steady-state assumption (i.e., $d[R]_w/dt = 0$):

$$\frac{d[R]_w}{dt} = 2f_d k_d[I] + k_1\bar{n}_1\left(\frac{N_{t_1}}{V_w N_a}\right) + k_2\bar{n}_2\left(\frac{N_{t_2}}{V_w N_a}\right) - k_{a_1}[R]_w\left(\frac{N_{t_1}}{V_w N_a}\right) - k_{a_2}[R]_w\left(\frac{N_{t_2}}{V_w N_a}\right) - k_{tw}[R]_w^2 \tag{19}$$

where f_d is the initiator efficiency factor and k_{tw} is the aqueous termination rate coefficient. The positive terms in eq 19 account for an increase in radicals in the aqueous phase due to initiator decomposition and radical desorption from both particle populations while the negative terms account for aqueous phase radical loss due to absorption into both particle populations and mutual aqueous phase termination. The following paragraphs explain how the radical absorption, desorption, and termination rate coefficients were obtained.

The absorption rate of radicals into the particles, σ_i, can be written as the product of the absorption rate coefficient, k_{a_i}, and the aqueous phase radical concentration:

$$\sigma_i = k_{a_i}[R]_w \tag{20}$$

Currently, some controversy exists on how to obtain the absorption rate coefficient. The three principal theories that exist differ on the degree to which absorption is dependent on particle diameter: The collision model (Gardon, 1968) assumes entry is dependent on the particle surface area, the diffusion model (Ugelstad and Hansen, 1976) predicts entry depends on the particle diameter, but the propagation model (Maxwell et al., 1991) assumes that entry is not a function of diameter at all. Because each of these proposed mechanisms have supporting evidence and support from independent research, a conclusion as to which absorption mechanism is correct cannot be reached on the basis of previous research. For the purposes of this model, all three mechanisms are used and tested, an approach similar to the one taken by Asua and de la Cal (1991). The absorption rate coefficient is written as

$$k_{a_i} = k_{adj} D_{s_i}^{\alpha} \tag{21}$$

where k_{adj} is an adjustable parameter, D_{s_i} is the swollen particle diameter, and α is an integer taking on a value of 0, 1, or 2 depending on whether propagation (Maxwell et al., 1991), diffusion (Ugelstad and Hansen, 1976), or collision (Gardon, 1968) is chosen as the absorption mechanism, respectively. If the absorption mechanism is not assumed to depend on particle size ($\alpha = 0$), then the absorption rate coefficient for both populations is simply equal to the adjustable parameter, k_{adj}.

Although desorption of radicals from the particles is not as important as absorption or termination for this system, the mechanism is included in this model for completeness. The desorption rate coefficient, k_i, obtained from the work of Asua et al. (1989) can be written as

$$k_i = k_{fm}[M]_p \frac{K_{0_i}}{K_{0_i}\beta + k_p[M]_p} \tag{22}$$

where k_{fm} is the chain transfer rate coefficient, β is the probability that a desorbed single-unit monomeric radical reacts in the aqueous phase, and K_{0_i}, is the size dependent monomer radical desorption rate coefficient. Assuming a diffusion mechanism, Nomura (1982) has derived the following relation for K_{0_i}:

$$K_{o_i} = \frac{12 D_w/m_d D_{s_i}^2}{1 + 2D_w/m_d D_p} \tag{23}$$

where D_w and D_p are the diffusion coefficients of a monomeric radical in the aqueous phase and the polymer particles, respectively, and m_d is the partition coefficient for the radical between these two phases.

Obtaining a proper function for the radical termination rate coefficient, k_t, is important because it will enable an accurate prediction of the gel effect. Investigations (Soh and Sundberg, 1982) based on bulk polymerization kinetics have provided a means to describe termination through a first principles approach. However, models based on this approach do not fit experimental data at higher conversions very well, precisely where radical termination may have the greatest influence. On the other hand, an empirical approach, although not as general, can provide a better prediction.

Hawkett et al. (1981) used an empirical relation to fit their own k_t versus W_p data. The resulting exponential function is

$$k_t = k_{t_0} \exp(-19.0 W_p^{2.1}) \tag{24}$$

However, inspection of the fit (dashed line of Figure 3) reveals that this relationship performs poorly at predicting higher conversion data ($W_p > 0.75$) by more than an order of magnitude. The poor fit of this equation in this area suffers from the same problem associated with the more rigorous models. This problem is resolved by

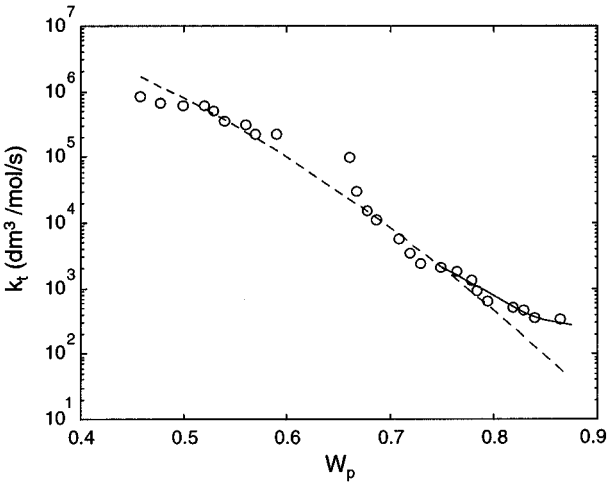

Figure 3. Radical termination rate coefficient relation. Exponential fit (dashed line) (Hawkett et al., 1981); polynomial addition (solid line).

Table 1. Physical and Chemical Parameter Values and Literature Sources Used in the Dynamic Competitive Growth Model

parameter	value	reference
k_d	1.3×10^{-6} s^{-1}	Penboss et al., 1986
k_{p_o}	253 dm^3/mol/s	Hawkett et al., 1981
B	0.1275	Sudol, 1983
ν_{fmc}	0.0383	Sudol, 1983
ν_{fm}	0.143	Soh and Sundberg, 1982
ν_{fp}	0.02	Soh and Sundberg, 1982
k_{t_o}	6.8×10^7 dm^3/mol/s	Hawkett et al., 1981
f_d	0.7	Li and Brooks, 1993
k_{fm}	2.7×10^{-5} dm^3/mol/s	Asua and de la Cal, 1991
β	0.3	Asua et al., 1989
D_w	5.0×10^{-6} cm^2/s	Asua et al., 1989
D_p	5.0×10^{-6} cm^2/s	Asua et al., 1989
m_d	1600	Asua et al., 1989
k_{tw}	7.0×10^7 dm^3/mol/s	Penboss et al., 1986
ρ_m	879.3 g/dm^3	James et al., 1989
ρ_p	1042.1 g/dm^3	Brandrup and Immergut, 1989

refitting the original data with a polynomial in the questionable area. Below a W_p of 0.75, eq 24 is used, but above this value, the following polynomial fitted to the data is used:

$$k_t = (-0.707 \times 10^6)W_p^3 + (1.886 \times 10^6)W_p^2 - (1.675 \times 10^6)W_p + 0.496 \times 10^6 \quad (25)$$

The improvement of this procedure is shown in Figure 3 where the dashed line is the exponential curve and the solid line is the polynomial addition.

Attention must be given to the methodology used to obtain the kinetic constants in the model. The approach used in this work was to choose kinetic constants from the work of researchers whose experimental systems were as similar as possible to the system studied here. The work of Hawkett et al. (1981) meets this requirement (styrene, 50 °C, seeded system, Interval III kinetics), for instance, and so the propagation rate coefficient at zero conversion, k_{p0}, and the termination rate coefficient at zero conversion, k_{t0}, obtained in that work are used here. The rest of the kinetic parameters, summarized in Table 1, were chosen in a similar manner.

Model Solution and Outputs. The set of ODEs along with the associated algebraic equations was integrated using LSODE contained in the program ODESSA (Leis and Kramer, 1988). In this work, the important simulation outputs are the evolution of the weight fraction polymer inside the particles, W_p, the average number of radicals per particle for each population, $\bar{n}_1$ and $\bar{n}_2$, the unswollen population diameters, D_1 and D_2, and, of course, their ratio, D_2/D_1.

To obtain W_p, the monomer concentration inside the particles, $[M]_p$, must first be determined. This is done by dividing the calculated dependent variable of eq 8 by V_p, the dependent variable in eq 7. W_p can then be calculated by

$$W_p = \frac{1/([M]_p(\mathrm{MW}_m)) - 1/\rho_m}{1/\rho_p + 1/([M]_p(\mathrm{MW}_m)) - 1/\rho_m} \quad (26)$$

The instantaneous fractional conversion, excluding the initial amount of polymer in the seed, depends on W_p in the following manner:

$$X = \frac{W_p(M_0 + M_{add} + P_0) - P_0}{M_0 + M_{add}} \quad (27)$$

where M_{add} is the total mass of monomer fed to the reactor up to the current time (solution of eq 10) and M_0, the initial monomer mass, is equal to $[M]_p V_p(\mathrm{MW}_m)$ at the start of the reaction.

The average number of radicals per particle for each population, $\bar{n}_i$, are easily obtained by solution of the balances represented by eq 17. Each population's unswollen diameter, D_i, is calculated with eq 30 (below) once V_{p_1} and V_{p_2} are determined via the following equations:

$$V_{p_1} = \frac{N_{t_1} V_p}{N_{t_1} + N_{t_2}(D_2/D_1)^3} \quad (28)$$

$$V_{p_2} = V_{p_1} N_{t_2}/N_{t_1}(D_2/D_1)^3 \quad (29)$$

$$D_i = 1.0 \times 10^8 \left[\frac{6.0 V_{p_i}}{\pi N_{t_i}}(1.0 - \phi_m)\right]^{1/3} \quad (30)$$

The unswollen particle diameter is tracked here instead of the monomer-swollen diameter primarily because the on-line particle size measurement used in this work measures unswollen particle diameters. Further arguments for using the unswollen diameters are given elsewhere (Poehlein and Vanderhoff, 1973).

Model Validation

Automated Reactor Control Facility. The preceding model was validated with data from a custom-built automated emulsion polymerization control facility. A detailed account of the capabilities of the facility, shown in Figure 4, is given elsewhere (Liotta, 1996; Liotta et al., 1997) and will not be repeated here. Instead, a brief description of the facility is presented below.

All reactions take place in a 3 L jacketed glass vessel. Adequate agitation in the reactor is provided by a stirrer containing two pitched blade impellers and four baffles welded to the interior surface of a cylindrical cooling coil. The proper reaction environment is also ensured by flowing nitrogen gas into the reactor. Isothermal conditions in the reactor are obtained with a temperature control system comprised of thermocouples, a cooling loop, and a hot water bath. A cascade temperature controller maintains the reactor temperature at

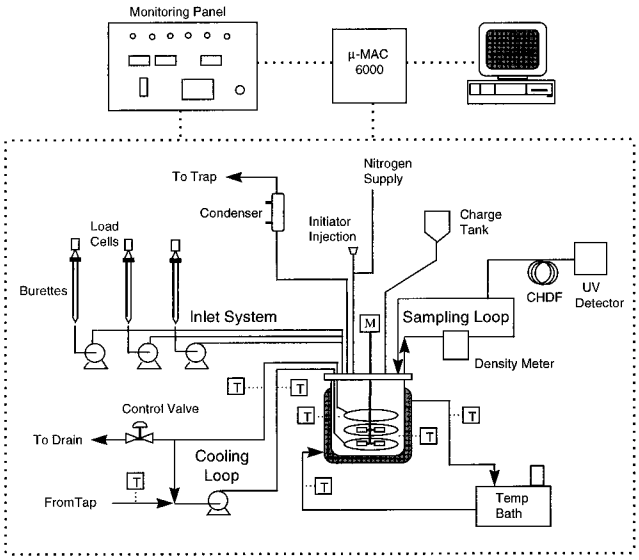

Figure 4. Automated reactor control facility schematic.

Table 2. Reaction Conditions for the Bidisperse Runs

reaction code	initial W_p	M_{add} (g)	F_m (g/min)	N_{t_1}	N_{t_2}
BD1	0.52	237	1.04	6.83×10^{16}	1.29×10^{16}
BD2	0.70	85	0.72	4.63×10^{16}	1.25×10^{16}
BD3	0.70	144	0.83	4.63×10^{16}	1.25×10^{16}
BD4	0.86	246	0.96	6.83×10^{16}	5.53×10^{15}

an operator-specified temperature by manipulating a control valve in the cooling loop. Semi-batch operation is made possible by the inlet flow system. The monomer is delivered to the reactor by reciprocating piston pumps, and its flow is measured by load cells. A flow controller based on the load cell measurement is implemented. A sampling loop carries the latex to an on-line density meter and an on-line particle size sensor. The density meter provides conversion information on an almost continuous basis. The particle size sensor, an on-line adaptation of capillary hydrodynamic fractionation (CHDF) (Silebi and DosRamos, 1988), is capable of measuring particle diameter every 10 min. Hardware and software are arranged in an intelligence hierarchy to provide data acquisition and control. Process apparatus are at the lowest level of the hierarchy while a host PC is at the top level. Communication between these two is made possible with a μMAC 6000, a front-end device. Software running on both the μMAC and PC allow for multitasking operation, historical data collection, prioritized interrupts, low-level and high-level control, and timed process automation.

Experimental Conditions. Validation experiments were run in the reactor control facility. A bidisperse system composed of 93 and 215 nm (in diameter) monodisperse seed populations (Dow Chemical) was grown under a variety of conditions. In addition to varying the flow of the monomer to the reactor, the initial W_p and the total amount of monomer fed to the reactor were changed from run to run. Table 2 lists the important process variables. The number of particles of each population were determined by gravimetry, and all the particles were assumed to be spherical.

All the bidisperse reactions were run with an initiator (potassium persulfate) concentration of 10 mM and an equivalent mass of buffer (sodium bicarbonate). Also, an initial added surfactant (sodium lauryl sulfate) concentration of 8 mM was used. Although this amount served to stabilize the particles initially, it was not sufficient for the entire reaction. To improve particle stability, particularly at later reaction times, the surfactant was added in small doses during the polymerization. An off-line calculation was performed to determine a surfactant metering schedule which would maintain a surface coverage of approximately 80%. The amount of added material to the reactor was minimized by feeding a concentrated surfactant solution.

In all cases, the reaction was allowed to proceed only when the monomer was being fed, so that when the monomer supply was depleted, all reactions were terminated. All polymerizations were carried out at a constant 50 °C under an atmospheric nitrogen environment using a stirrer speed of 450−500 RPM.

On-line measurements were taken in the facility to monitor the progress of the emulsion polymerization. Reactor temperature was monitored to ensure that the temperature controller maintained isothermal conditions at 50 ± 0.5 °C. A load cell tracked the amount of monomer fed and the monomer feed rate from a hanging burette. On-line density measurements were also taken to provide information on the extent of reaction. Both W_p and X were calculated from the frequent density measurements. On a less frequent time scale (10 min), the on-line CHDF provided measurements of unswollen particle diameter for each population.

Table 3. Bidisperse Model Validation Results Using W_p and D_2/D_1 Data for BD1−BD4

absorption model	k_{adj}	SSE (W_p)	SSE (D_2/D_1)
propagation ($\alpha = 0$)	1.9×10^6	0.078	4.65
diffusion ($\alpha = 1$)	1.1×10^{11}	0.080	3.36
collision ($\alpha = 2$)	5.5×10^{15}	0.068	2.69

Validation Results. Experimental data from the on-line sensors were used to validate the dynamic bidisperse growth model. Simulations results, obtained using the information specified in Table 2, and the initial condition, $\bar{n}_{1_0} = \bar{n}_{2_0} = 0$, were compared to the experimental results. Specifically, simulated W_p and D_2/D_1 values were fit to the corresponding experimental outputs. These two data sets were used in the analysis because the two sensors used to obtain the data (W_p and D_2/D_1) provide independent information that can be used to validate the model. For both data sets, only one adjustable parameter, k_{adj}, located in the radical absorption equation was varied to produce a minimum sum of the squared error (SSE) between the experimental points and simulated values. During this calculation, priority was given to W_p data because this data is more sensitive to changes in k_{adj} than D_2/D_1 data. Because there were three forms of the radical absorption mechanism, and thus three potential models, an SSE calculation was performed for each model. The results for both data sets (W_p and D_2/D_1) are shown in Table 3. The results for the W_p data show that the fit for the collision model ($\alpha = 2$) is significantly better (~15%) than the models assuming a propagation or diffusion mechanism for radical absorption. Further proof supporting the collision model is obtained from the diameter ratio results where the collision model is 42% better than the propagation model and 20% better than the diffusion model. An example of the fit with all three models for one experiment is shown in Figure 5. Bidisperse run BD4 is used in this plot because it provides the largest difference between the predictions of the three models. As expected from the SSE calculations, the collision model does a much better job of predicting the dynamic competitive growth behavior.

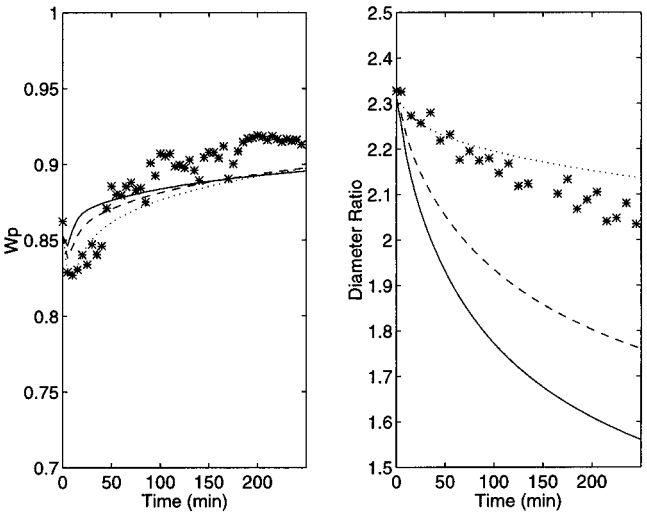

Figure 5. Example fits of the propagation model (solid line), diffusion model (dashed line), and collision model (dotted line) to W_p data (left plot) and D_2/D_1 data (right plot) of reaction BD4.

In their work, Asua and de la Cal, [Asua and de la Cal, 1991] showed that, for a monodisperse system, both the collision and diffusion model were incompatible with the assumption that the desorption of radicals occurs through a diffusion mechanism, the assumption used here. Unlike our results, they concluded that only the propagation absorption model could explain the fractional conversion data they obtained from other work (Hawkett et al., 1980; Penboss et al., 1986). They are cautious about this conclusion, however, and admit that a limited amount of data was used with a rather small range of particle sizes. This observation brings up an important point. It is unlikely that seeded unimodal emulsion polymerizations can be used to draw an unambiguous conclusion about the correct absorption mechanism. Competitive growth experiments, on the other hand, provide data for two different-sized populations under equivalent conditions, a richer data set that can be used to better distinguish between size-dependent mechanistic suppositions.

Although the collision model is superior at predicting the competitive growth data, Figure 5 shows that it slightly underestimates the relative narrowing of the bidisperse system. A still better fit of the data can be obtained by varying α and refitting k_{adj} to obtain a minimum (D_2/D_1) SSE. An SSE of 2.47 is obtained for $\alpha = 1.85$ and $k_{adj} = 1.05 \times 10^{15}$. These values are used in all subsequent plots and bidisperse model calculations.

Analysis of Experimental and Simulated Results

Weight Fraction Polymer in the Particles. The reaction dynamics of the bidisperse system can be investigated by studying the dynamics of W_p. The experimental points are compared to the best model fit ($\alpha = 1.85$ and $k_{adj} = 1.05 \times 10^{15}$) in Figure 6. The model does an adequate job of predicting the effect of the changing process conditions on W_p.

The low W_p run (BD1) of Figure 6 exhibits pseudo-steady-state characteristics. The feed rate, in this case, is high enough to maintain a relatively low W_p value throughout the run. This constant monomer concentration is a result of a near-constant reaction rate which is due to the relatively constant $\bar{n}$ values in both particle populations. Figure 7 shows the simulated $\bar{n}$ trajectories of the bidisperse system for this run (BD1). The smaller particles are close to maintaining Smith-Ewart (S-E) case 2 kinetics ($\bar{n} = 0.5$) throughout the run while the larger particles maintain a slightly higher average number of radicals.

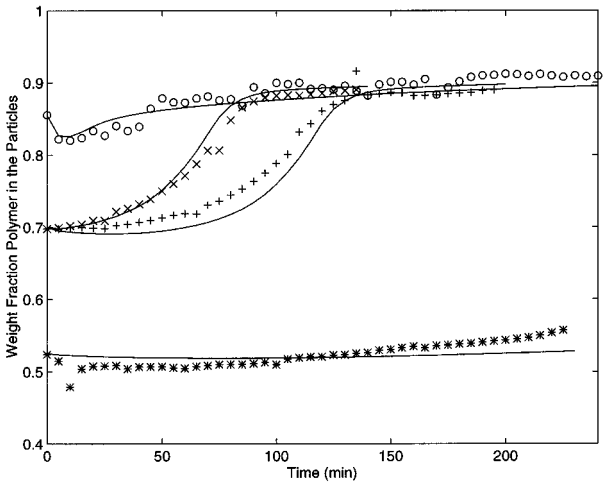

Figure 6. Weight fraction polymer inside the particles calculated from densitometer data (points) and best fit model (lines) for reactions BD1 (*), BD2 (×), BD3 (+), and BD4 (○).

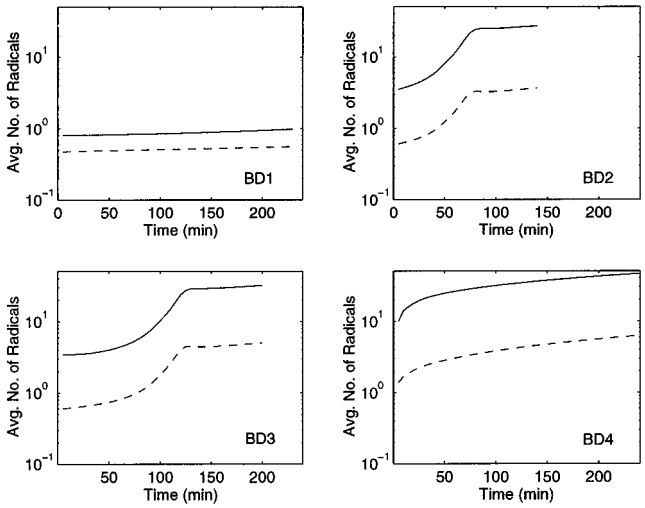

Figure 7. Average number of radicals per particle for D_1 (dashed line) and D_2 (solid line) populations obtained from the best fit model for reactions BD1−BD4.

The high W_p run (BD4) in Figure 6 has a similar feed flow rate as in BD1 and results in similar dynamics. However, the reaction kinetics are much different. This can be seen in the $\bar{n}$ curves of Figure 7. The larger particles are clearly in S-E case 3 regime ($\bar{n} \gg 0.5$) while the smaller particles are in transition from S-E case 2 to case 3 conditions. Although these $\bar{n}$ values are increasing with time (particularly $\bar{n}_2$), W_p remains relatively constant throughout the run, an indication of a constant reaction rate. The rate is constant in this case because a diffusion limitation on propagation causes k_p to drop and offset the increase in $\bar{n}_1$ and $\bar{n}_2$.

The intermediate W_p runs (BD2 and BD3) in Figure 6 exhibit the most interesting behavior. This is because these runs go through a transition leading to an autoacceleration of the rate. At early reaction times, the reaction rate is low enough that a balance is achieved between monomer feed and monomer disappearance due to the reaction, similar to run BD1. At some critical point, however, both runs transition to the gel effect regime. The consequence is an autoaccelera-

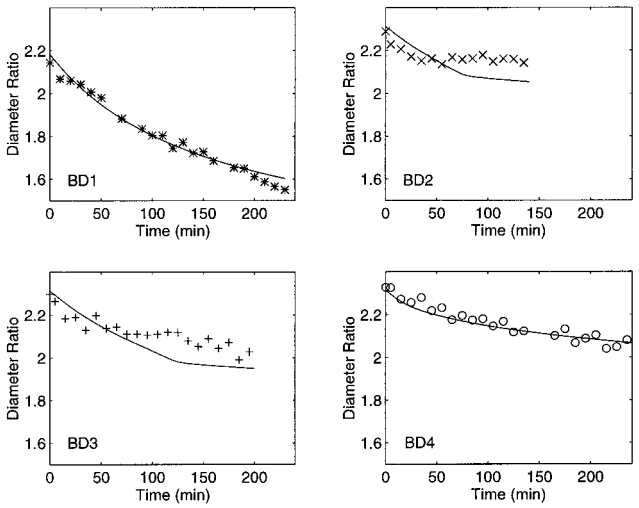

Figure 8. Particle diameter ratios obtained from on-line CHDF (points) and a best fit model (lines) for reactions BD1 (*), BD2 (×), BD3 (+), and BD4 (○).

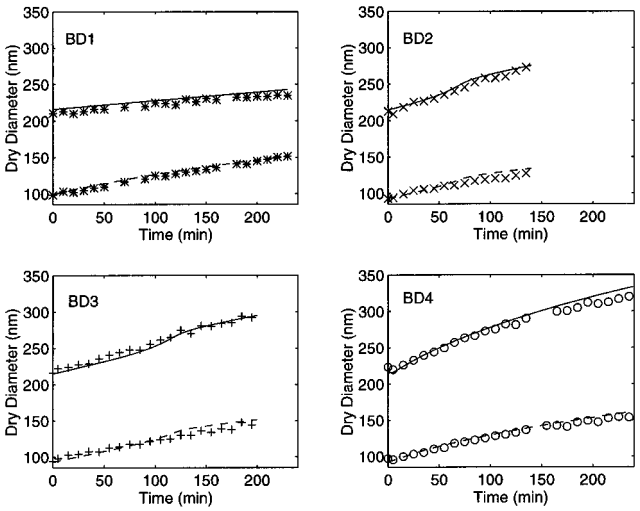

Figure 9. Unswollen particle diameters, D_1 (dashed line) and D_2 (solid line), obtained from on-line CHDF (points) and a best fit model (lines) for reactions BD1 (*), BD2 (×), BD3 (+), and BD4 (○).

tion of the rate until the limiting conversion previously described is reached. This phenomenon is also quite clear in the $\bar{n}$ curves of Figure 7. For both runs, the smaller particles transition from S-E case 2 to case 3 kinetics while the larger particles, already in that transition region, become firmly entrenched in S-E case 3 kinetics.

The conclusion from Figures 6 and 7 is that similar monomer feed rates yield different system dynamics and reaction kinetics depending on the degree to which the particle is swollen by the monomer. The impact of W_p on the dynamics of particle growth is made even more clear by considering the time evolution of the particle diameters and, more importantly, the evolution of the diameter ratio, discussed in the following section.

Particle Diameter Ratio and Diameter Evolution. The evolution of the diameter ratio with the changing process conditions of BD1−BD4 is discussed in the next several paragraphs. Figure 8 compares the on-line CHDF data to the simulated results on four plots with the same scale. Keeping W_p at a low value (BD1) enables smaller particles to grow at a relatively fast rate when compared to larger particles, thus leading to a large relative narrowing effect. The plot for the average number of radicals per particle in these populations (Figure 7) explains this phenomenon. The ratio of $\bar{n}_2/\bar{n}_1$ is low for this run, and so both populations have similar volume growth rates. This results in the smaller particles approaching the larger particles in diameter. The model adequately tracks this narrowing effect.

The high W_p run of Figure 8 (BD4) results in a different diameter ratio evolution. The relative narrowing is reduced in this run due to larger $\bar{n}_2/\bar{n}_1$ values. The $\bar{n}$ curves for run BD4 in Figure 7 show that this run has larger $\bar{n}_2/\bar{n}_1$ ratios than those in run BD1. The $\bar{n}_2/\bar{n}_1$ ratio in BD4 approaches a value of 8 near the end of the run. Since the diameter ratio remains above 2 in this run, this $\bar{n}_2/\bar{n}_1$ ratio is not large enough to allow for relative broadening as determined by the condition of eq 4.

The two runs started at a W_p of 0.7 (BD2 and BD3) show a change in competitive growth characteristics midway through the run. A decrease in relative narrowing is evident in conjunction with the start of the autoacceleration phenomenon in each run. Once again the $\bar{n}$ curves provide the reasoning behind this relative growth change. Since autoacceleration is size-dependent, large particles have a greater increase in the average number of radicals than the smaller particles. This leads to an increase in the $\bar{n}_2/\bar{n}_1$ ratio which decreases the relative narrowing effect. Also evident for these runs is a slight mismatch between the model and the experimentally obtained diameter ratios after the start of the autoacceleration of the rate. This mismatch is best explained by analyzing the growth of the individual monodisperse populations.

The evolution of the individual population diameters is shown in Figure 9. As expected from the diameter ratio results, the model adequately tracks the diameter evolution in both populations. One interesting note is that the source of the mismatch for the intermediate results is shown in Figure 9 as a slight overestimate of the growth rate of the smaller particles. The probable cause of this overestimate is that the modeled $\bar{n}_1$ moves out of S-E case 2 conditions too early.

Reachable Regions. The objective in this section is to obtain the limits of the influence of process conditions on competitive growth. We start with a definition to aid in the realization of the above objective. For nonlinear continuous time systems, Stengel (1986) defines a reachable region as the envelope of final states that can be reached from an initial state through the use of available control action. Applied to this system, the reachable region is the envelope of diameter ratios that can be attained starting from an initial point with a certain diameter ratio, particle diameters, and other conditions.

In this system, feedback control is not required to obtain the reachable region. Simulations of the validated model confirm the general trend presented in Figure 2. That is, the limiting diameter ratios are obtained by running the polymerizations at the upper and lower limits of W_p. Using the conditions of run BD3, the following example illustrates this point. For maximum narrowing (lowest D_2/D_1 trajectory), W_p should be as low as possible during the run. This is easily accomplished by preswelling the latex with all the monomer in the recipe and running a strictly batch reaction. Using the conditions of BD3, the monomer amount in the recipe is just short of reaching the monomer saturation limit of the particles.

Alternatively, for the minimum amount of narrowing (highest D_2/D_1 trajectory), W_p should be at the highest

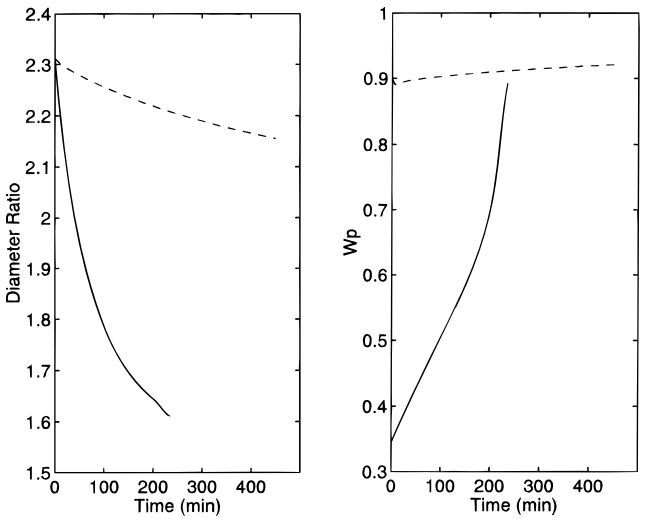

Figure 10. The limits of the reachable region (left) and corresponding W_p trajectories (right) for reaction BD3.

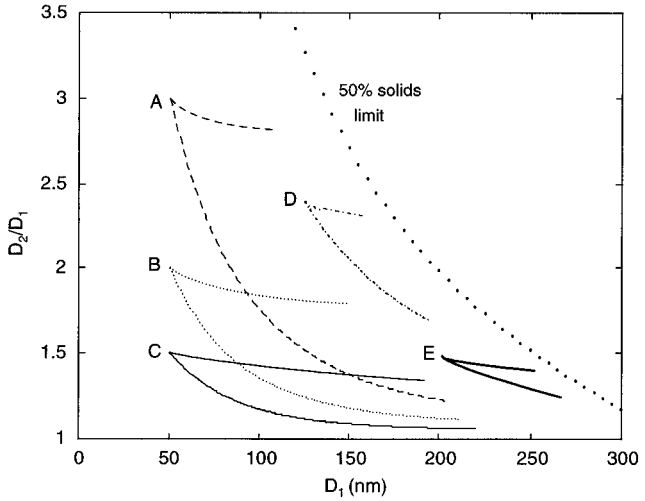

Figure 11. Reachable regions for several initial diameter pairs. $D_1 = 50$ nm, $D_2 = 150$ nm (region A); $D_1 = 50$ nm, $D_2 = 100$ nm (region B); $D_1 = 50$ nm, $D_2 = 75$ nm (region C); $D_1 = 125$ nm, $D_2 = 300$ nm (region D); $D_1 = 200$ nm, $D_2 = 300$ nm (region E).

practical value. Emphasis is on the word practical because as W_p values increase in the limiting conversion region, the reaction rate decreases exponentially. To sustain the reaction at a high W_p for this system (>0.92), the corresponding monomer feed rate would have to be very low, which would result in a very long reaction. A reasonable value for W_p for run BD3 is 0.9. A slow constant monomer feed rate of 0.35 g/min will maintain the W_p around this value for the remainder of the run. The resulting W_p trajectories and reachable region are shown in Figure 10.

Any part of the region outlined by the two diameter ratio trajectories can be reached by simply varying W_p during the reaction. As presented earlier, the monomer feed rate is an effective way to change W_p.

Using the same approach, Figure 11 shows the simulation results of reactions run at the lower and upper W_p limits for several initial unswollen diameter pairs. In this case, the simulations were run using the initial reaction conditions listed in Table 4. Also, the diameter ratios are plotted versus the smaller population size instead of time. All the initial populations were grown with 400 g of monomer to a final conversion of 90%. This amount was chosen so that the various cases

Table 4. Simulated Reaction Conditions for Determining the Reachable Regions

initial conditions	reaction conditions
$[I]_0 = 0.01$ mol/dm^3	$N_{t_1} = N_{t_2} = 2.5 \times 10^{16}$
$\bar{n}_{1_0} = \bar{n}_{2_0} = 0.0$	$V_w = 1.0$ dm^3

were kept from exceeding the practical reaction limit of 50% solids.

The bounded regions of Figure 11 represent the practical reachable regions of the respective diameter starting points. Comparison of region B of Figure 11 with Figure 1 shows that the order of volume growth, c, for this system can be varied between 1 and ~2.7. The important conclusion from this is that, given similar conditions, operating the reactor in semi-batch allows one to change the order of volume growth by changing W_p (via F_m) during the reaction. This is an improvement over the constant order of volume growth found by Vanderhoff and co-workers (Vanderhoff and Bradford, 1956; Vanderhoff et al., 1956) in a batch reactor. Therefore, unlike the situation in a batch reactor, relative particle growth can be varied in a semi-batch reactor. Ways to influence the reachable region are discussed in the following paragraphs.

Since particles cannot be "unpolymerized", these regions can extend only to the right of each starting point. The effect of changing the initial diameter ratio on the size of the reachable region is demonstrated in Figure 11 by the three diameter pairs using 50 nm particles for the smaller population (regions A, B, and C). As D_2/D_1 increases, the size of the region also increases. This is due to the fact that populations can only experience relative narrowing via the growth mechanism. Thus, the larger the particle diameter ratio, the larger the potential to alter the initial relative size.

Reachable regions are also influenced by the magnitude of the initial diameter pairs. Region E in Figure 11 has the same initial diameter ratio as region C, yet it bounds a smaller area in the D_2/D_1 vs D_1 plane. The reason for this is that the relative narrowing effect diminishes as particles get larger. As explained previously, the greatest relative narrowing (in terms of diameter) occurs at $\bar{n}_1 = \bar{n}_2$. As both particles become larger (greater than 200 nm), the difference between $\bar{n}_1$ and $\bar{n}_2$ at the monomer saturation limit for the two different-sized particles becomes greater. In equivalent terms, the slope of the line corresponding to a W_p value of 0.4 in Figure 2 will eventually increase as particle diameter increases.

On the basis of these results, equivalent conclusions can be made for distributions of particles that have initial diameter characteristics located in between the initial diameter pairs depicted in Figure 11. For this system, the growth mechanism can essentially be used only to relatively narrow diameter distributions. The broader the initial distribution, the more potential there is to alter the initial relative breadth.

Conclusions

A study of the dynamics of bidisperse particle growth was presented in this paper. The relative diameter growth of a bidisperse system is expected to be representative of the relative growth characteristics of a more general distribution. The evolution of the diameter ratio of the system, a relative growth indicator, under a variety of process conditions was studied in a combined

theoretical and experimental investigation. The contributions of this work are outlined below.

(1) A dynamic bidisperse particle growth model was developed using recent advances in radical diffusion and kinetics. The model outputs included weight fraction polymer in the particles, W_p, unswollen particle diameter, D, and diameter ratio, D_2/D_1. The bidisperse model was validated with data from several semi-batch polymerizations performed in an automated reactor control facility. The experimental validation showed that, of the three most probable radical absorption mechanisms, only the collision absorption mechanism adequately fits the W_p and D_2/D_1 data. The bidisperse model validation showed that competitive growth experiments provide a rich data set that can be used to distinguish between competing absorption mechanisms.

(2) Using the validated model as a tool, growth was determined to be a suitable manipulatable mechanism for particle size control. It was shown that, unlike batch reactions which were limited to a single diameter ratio trajectory, running the reaction in semi-batch opened this trajectory into an envelope, the reachable region. Reachable regions were specified for different initial diameter ratios by running simulations at the practical upper and lower W_p limits. The areas of these regions were shown to depend on the magnitude of the initial diameter ratio and the individual particle diameters.

Nomenclature

B: Empirical constant in k_p expression
c: Order of volume growth
D: Unswollen particle diameter (nm)
D_p: Polymer phase radical diffusion coefficient (cm^2/s)
D_s: Swollen particle diameter (cm)
D_w: Aqueous phase radical diffusion coefficient (cm^2/s)
f: Parameter described by eq 18
f_d: Initiator efficiency factor
F_m: Monomer feed rate (mol/s)
$[I]$: Initiator concentration (mol/dm^3)
k: Radical desorption rate coefficient (s^{-1})
k_a: Radical absorption rate coefficient ($dm^3/mol/s$)
k_{adj}: Adjustable parameter defined by eq 21
k_d: Initiator decomposition rate coefficient (s^{-1})
k_{fm}: Monomer chain transfer constant ($dm^3/mol/s$)
k_p: Propagation rate coefficient ($dm^3/mol/s$)
k_{p_0}: Propagation rate coefficient at zero conversion ($dm^3/mol/s$)
k_t: Termination rate coefficient ($dm^3/mol/s$)
k_{t_0}: Termination rate coefficient at zero conversion ($dm^3/mol/s$)
k_{tw}: Aqueous termination rate coefficient ($dm^3/mol/s$)
K_a, K_b: Proportionality constants
K_0: Monomer radical diffusion rate (s^{-1})
m_d: Radical partition coefficient
M_{add}: Mass of added monomer at any time (g)
M_0: Initial monomer mass (g)
$[M]_p$: Monomer concentration in the particles (mol/dm^3)
$[M]_w$: Monomer concentration in the aqueous phase (mol/dm^3)
$[M]_{sat}$: Monomer concentration in the aqueous phase at saturation (mol/dm^3)
MW_m: Molecular weight of monomer (g/mol)
$\bar{n}$: Average number of radicals per particle
N_a: Avogadro's number
N_t: Total number of particles
P_0: Initial polymer mass (g)
r: Swollen particle radius (μm)
R_g: Gas constant (J/mol/K)
R_p: Polymerization rate ($mol/dm^3/s$)
$[R]_w$: Aqueous phase radical concentration (mol/dm^3)
t: Time (s)
T: Temperature (°C)
$T°$: Temperature (K)
V: Unswollen particle volume (nm^3)
v_f: Particle free volume
v_{fm}: Monomer contribution to particle free volume
v_{fp}: Polymer contribution to particle free volume
v_{fmc}: Critical particle free volume
V_p: Total particle population volume (dm^3)
V_r: Reaction medium volume (dm^3)
V_s: Swollen particle volume (dm^3)
V_w: Water volume (dm^3)
W_p: Weight fraction polymer in the particles
X: Instantaneous fractional conversion

Greek Variables

α: Radical absorption dependency on particle diameter
α_a: Dimensionless radical absorption term
β: Probability of aqueous phase radical reaction
γ: Interfacial tension (dyn/cm)
ρ_m: Monomer density (g/dm^3)
ρ_p: Polymer density (g/dm^3)
ϕ_m: Monomer volume fraction in particles
σ: Radical absorption rate (s^{-1})
χ: Flory−Huggins interaction parameter

Literature Cited

Asua, J. M.; de la Cal, J. C. Entry and Exit Rate Coefficients in Emulsion Polymerization of Styrene. *J. Appl. Polym. Sci.* **1991**, *42*, 1869−1877.

Asua, J. M.; Sudol, E. D.; El-Aasser, M. S. Radical Desorption in Emulsion Polymerization. *J. Polym. Sci., Part A: Polym. Chem.* **1989**, *27*, 3903−3913.

Brandrup, J.; Immergut, E. *Polymer Handbook*, 3rd ed.; Wiley: New York, 1989.

Chen, S.; Wu, K. Emulsion Polymerization: On the Characterization of the Particle Size Distribution. *J. Polym. Sci., Part A: Polym. Chem.* **1988**, *26*, 1143−1155.

Gardon, J. L. Emulsion Polymerization. I. Recalculation and Extension of the Smith-Ewart Theory. *J. Polym. Sci., Part A-1* **1968**, *6*, 623−641.

Hawkett, B. S.; Napper, D. H.; Gilbert, R. G. Seeded Emulsion Polymerization of Styrene. *J. Chem. Soc., Faraday Trans. 1* **1980**, *76*, 1323−1343.

Hawkett, B. S.; Napper, D. H.; Gilbert, R. G. Analysis of Interval III Kinetic Data for Emulsion Polymerizations. *J. Chem. Soc., Faraday Trans. 1* **1981**, *77*, 2395−2404.

James, D. H.; Gardner, J. B.; Mueller, E. C. In *Encyclopedia of Polymerization Science and Technology*; Mark, H. F., Ed.; Wiley: New York, 1989.

Leis, J. R.; Kramer, M. A. The Simultaneous Solution and Sensitivity Analysis of Systems Described by Ordinary Differential Equations. *ACM Trans. Math. Soft.* **1988**, *23* (1), 45−60.

Li, B.; Brooks, B. W. Prediction of the Average Number of Radicals per Particle for Emulsion Polymerization. *J. Polym. Sci., Part A: Polym. Chem.* **1993**, *31*, 2397−2402.

Liotta, V. *Control of Relative Particle Growth in Emulsion Polymerization*. Ph.D. Dissertation, Lehigh University, Bethlehem, PA, 1996.

Liotta, V.; Sudol, E. D.; El-Aasser, M. S.; Georgakis, C. On-line Monitoring, Modeling, and Model Validation of Semi-Batch Emulsion Polymerization in an Automated Reactor Control Facility. Submitted to *J. Polym. Sci.*, 1997.

Maxwell, I. A.; Morrison, B. R.; Napper, D. H.; Gilbert, R. G. Entry of Free Radicals into Latex Particles in Emulsion Polymerization. *Macromolecules* **1991**, *24*, 1629−1640.

Mork, P. C. Kinetics of Competitive Polymerization in Bidisperse Seed Systems Using Oil-Soluble Initiators: Calculation of Effect of Various Dimensionless Parameters. *J. Polym. Sci., Part A: Polym. Chem.* **1995**, *33*, 2305−2316.

Morton, M.; Kaizerman, S.; Altier, M. W. Swelling of Latex Particles. *J. Colloid Sci.* **1954**, *9*, 300−312.

Nomura, M. In *Emulsion Polymerization*; Piirma, I., Ed.; Academic Press: New York, 1982.

Penboss, I. A.; Gilbert, R. G.; Napper, D. H. Entry Rate Coefficients in Emulsion Polymerization Systems. *J. Chem. Soc., Faraday Trans. 1* **1986**, *82*, 2247−2268.

Poehlein, G.; Vanderhoff, J. W. Competitive Growth of Polystyrene Latex Particles: Theory and Growth. *J. Polym. Sci.* **1973**, *11*, 447−452.

Silebi, C. A.; DosRamos, J. G. Separation of Submicrometer Particles by Capillary Hydrodynamic Fractionation (CHDF). *J. Colloid Interface Sci.* **1988**, *130*, 14−24.

Soh, S. K.; Sundberg, D. C. Diffusion-Controlled Vinyl Polymerization. IV. Comparison of Theory and Experiment. *J. Polym. Sci., Polym. Chem. Ed.* **1982**, *20*, 1345−1371.

Stengel, R. *Stochastic Optimal Control, Theory and Application*; John Wiley & Sons: Princeton, NJ, 1986.

Sudol, E. D. *Kinetics of Successive Seeding of Monodisperse Latex*. Ph.D. Dissertation, Lehigh University, Bethlehem, PA, 1983.

Sundberg, D. C.; Hseih, J. Y.; Soh, S. K.; Baldus, R. F. Diffusion-Controlled Kinetics in the Emulsion Polymerization of Styrene and Methyl Methacrylate. *Emulsion Polymers and Emulsion Polymerization*; Bassett, D. R., Hamielec, A. E., Eds.; ACS Symposium Series 165; American Chemical Society: Washington, DC, 1981; pp 327−343.

Ugelstad, J.; Flogstad, H.; Hansen, F. K.; Ellingsen, T. Kinetics and Mechanism of Emulsion Polymerization. *J. Polym. Sci., Part C* **1973**, *42*, 473−485.

Ugelstad, J.; Hansen, F. K. Kinetics and Mechanism of Emulsion Polymerization. *Rubber Chem. Technol.* **1976**, *49* (3), 536−609.

Vanderhoff, J. W.; Bradford, E. B. An Investigation of the Mechanism and Kinetics of Emulsion Polymerization by Electron Microscopy. *Tech. Assoc. Pulp Pap. Ind.* **1956**, *39* (9), 650−656.

Vanderhoff, J. W.; Bradford, E. B.; T. Alfrey, J. Some Factors Involved in the Preparation of Uniform Particle Size Latexes. *J. Polym. Sci.* **1956**, *20*, 225−234.

Received for review October 11, 1996
Revised manuscript received May 9, 1997
Accepted May 13, 1997[⊗]

IE960643G

[⊗] Abstract published in *Advance ACS Abstracts,* July 1, 1997.